Monthly Notices of the ROYAL ASTRONOMICAL SOCIETY

MNRAS **437,** 3288–3297 (2014) doi:10.1093/mnras/stt2128
Advance Access publication 2013 December 4

Herschel observations of debris discs orbiting planet-hosting subgiants

Amy Bonsor,[1,2★] Grant M. Kennedy,[3] Mark C. Wyatt,[3] John A. Johnson[4] and Bruce Sibthorpe[5]

[1]*UJF-Grenoble 1/CNRS-INSU, Institut de Plantologie et d'Astrophysique de Grenoble (IPAG) UMR 5274, Grenoble F-38041, France*
[2]*School of Physics, H. H. Wills Physics Laboratory, University of Bristol, Tyndall Avenue, Bristol BS8 1TL, UK*
[3]*Institute of Astronomy, University of Cambridge, Madingley Road, Cambridge CB3 OHA, UK*
[4]*Harvard–Smithsonian Center for Astrophysics, 60 Garden Street, Cambridge MA 02138, USA*
[5]*SRON Netherlands Institute for Space Research, Zernike Building, PO Box 800, NL-9700 AV Groningen, the Netherlands*

Accepted 2013 October 31. Received 2013 October 29; in original form 2013 October 11

ABSTRACT

Debris discs are commonly detected orbiting main-sequence stars, yet little is known regarding their fate as the star evolves to become a giant. Recent observations of radial velocity detected planets orbiting giant stars highlight this population and its importance for probing, for example, the population of planetary systems orbiting intermediate mass stars. Our *Herschel*† survey observed a subset of the Johnson et al. program subgiants, finding that 4/36 exhibit excess emission thought to indicate debris, of which 3/19 are planet-hosting stars and 1/17 are stars with no current planet detections. Given the small numbers involved, there is no evidence that the disc detection rate around stars with planets is different to that around stars without planets. Our detections provide a clear indication that large quantities of dusty material can survive the star's main-sequence lifetime and be detected on the subgiant branch, with important implications for the evolution of planetary systems and observations of polluted or dusty white dwarfs. Our detection rates also provide an important constraint that can be included in models of debris disc evolution.

Key words: planets and satellites: general – infrared: planetary systems.

1 INTRODUCTION

Belts of rocks and dust, known as debris discs are commonly detected around main-sequence stars. Recent surveys found infrared (IR) excess emission, a good indicator for the presence of a debris disc, around 15 per cent of FGK stars and 32 per cent of A stars (Beichman et al. 2006; Bryden et al. 2006; Su et al. 2006; Moro-Martín et al. 2007; Hillenbrand et al. 2008; Trilling et al. 2008; Greaves, Wyatt & Bryden 2009). The observed emission must result from small dust grains (e.g. Wyatt 2008), yet, theoretical estimates find that the lifetime of such small grains against both collisions and radiative forces is short. The collisional evolution of a population of larger parent bodies is, therefore, generally invoked to explain the observed debris discs (Wyatt 2008). Such collisional evolution naturally explains the decay with age in the fractional luminosity of observed debris discs (e.g. Rieke et al. 2005; Su et al. 2006; Currie, Plavchan & Kenyon 2008).

As the number of resolved images of debris discs grow (e.g. Holland et al. 1998; Kalas, Graham & Clampin 2005; Smith et al. 2009; Churcher, Wyatt & Smith 2011a), so does the diversity of structures observed. In many cases, interactions with planets are invoked to explain the observations (e.g. Augereau et al. 2001; Augereau & Beust 2006; Chiang et al. 2009; Churcher et al. 2011b). It may be that the presence of debris discs correlates with the presence of planets, but there is as yet no strong evidence either way (Moro-Martín et al. 2007; Bryden et al. 2009; Kóspál et al. 2009; Wyatt et al. 2012). Theoretically, a correlation may be anticipated because the properties of the protoplanetary disc affect the outcome both for the debris disc and the planets (Wyatt, Clarke & Greaves 2007a), or because dynamical effects such as instabilities in the planetary system can also have a significant effect on the debris disc (Raymond, Scalo & Meadows 2007). This motivates observations of planets and debris discs orbiting the same stars.

The majority of confirmed planets are currently detected using the radial velocity (RV) technique.[1] RV detections of planets orbiting main-sequence A stars are hindered due to high jitter levels and rotationally broadened absorption lines (Galland et al. 2005; Lagrange et al. 2009). Thus, previous efforts to compare the populations of planets and debris discs have focused on sun-like stars and RV planets (Moro-Martín et al. 2007; Bryden et al. 2009;

★ E-mail: amy.bonsor@gmail.com

† *Herschel* is an ESA space observatory with science instruments provided by European-led Principal Investigator consortia and with important participation by NASA.

[1] exoplanet.eu.

Kóspál et al. 2009). There are now a growing number of detections of planets around 'retired' A stars, now on the subgiant or giant branch (e.g. Johnson et al. 2006, 2007; Bowler et al. 2010; Sato et al. 2010), although some controversy does exist regarding the exact evolutionary paths of these stars (Lloyd 2011, 2013; Schlaufman & Winn 2013). These observations provide some key insights into the potential differences between the planetary population around sun-like and intermediate-mass stars, that otherwise can only be probed by direct imaging of planets around main-sequence A stars (e.g. Kalas et al. 2008; Marois et al. 2008; Rameau et al. 2013). Very little, however, is known regarding the population of debris discs around subgiants. By studying debris discs orbiting these 'retired' A stars, we access a new population of planetary systems, from which more can be learnt regarding the structure and links between planets and debris discs, with a focus on intermediate-mass stars.

In addition to providing a new and interesting sub-set of planetary systems to study, debris discs orbiting subgiants also provide evidence regarding the first step in the evolution of debris discs beyond the main sequence. The interest in the fate of debris discs has grown with the growing evidence for planetary systems orbiting white dwarfs. Observations of both polluted (e.g. Zuckerman et al. 2010; Koester et al. 2011; Gänsicke et al. 2012) and dusty (e.g. Farihi, Jura & Zuckerman 2009; Barber et al. 2012) or gaseous (e.g. Gänsicke et al. 2006; Gänsicke, Marsh & Southworth 2007; Melis et al. 2010) material very close to white dwarfs are thought to be linked with the presence of planets and planetesimal belts (e.g. Debes & Sigurdsson 2002; Jura 2008; Bonsor, Mustill & Wyatt 2011; Debes, Walsh & Stark 2012). For this to be true, both planets and debris discs must survive the star's evolution from the main sequence to the white dwarf phase. The subgiant branch is the first step on this evolutionary path.

In this work, we present *Herschel* observations of a sample of 36 subgiants in which we search for excess emission, indicative of a debris disc. RV planets have been detected for half of the sample as part of the RV survey to search for planets orbiting 'retired' A stars using Lick and Keck observatories (Johnson et al. 2006), whilst the other half of the sample was observed as part of the same program, but no planets were detected. We start in Section 2 by discussing our *Herschel* observing strategy. This is followed in Section 3 by the results of our observations and a discussion of their meaning in Sections 4 and 5.

2 OBSERVATIONS

Observations were performed using the *Herschel* Photodetector and Array Camera and Spectrometer (PACS; Poglitsch et al. 2010) at 100 and 160 μm, as listed in Table 1. These observations were performed in mini scan-map mode with two observations being performed with a 40° cross-linking angle. Four repeats were used for each observation and with eight scan legs per repeat. The total observing time was approximately 1790 s per target.

Data were reduced with the Herschel Interactive Processing Environment version 7.0 Build 1931 (HIPE; Ott 2010) using version 32 of the PACS calibration. Some data from the telescope turn-around phase (when scanning above 5 arcsec s^{-1}) were used to minimize the ultimate noise level. Maps were then made using the HIPE *photProject* task to provide 'drizzle' maps (Fruchter & Hook 2002) with pixel scales of 1 and 2 arcsec in the 100 and 160 μm bands, respectively. The data were high-pass filtered to mitigate low-frequency $1/f$ noise, using filtering scales of 66 and 102 arcsec (equivalent to a filter radius of 16 and 25 PACS frames) in the 100 and 160 μm bands, respectively.

The PACS point spread function (PSF or beam) includes significant power on large scales (10 per cent beyond 1 arcmin). Consequently, the filtering performed during the data reduction will reduce the flux density of a source by 10–20 per cent, due to the filter removing the wings of the PSF. For point sources this can be readily accounted for using correction factors, determined from comparison of bright stars with known fluxes with the PACS aperture flux. Correction factors of 1.19 ± 0.05 and 1.21 ± 0.05 at 100 and 160 μm were determined from analysis of the Disc Emission via a Bias-free Reconnaissance in the Infrared/Submillimetre (DEBRIS) survey (e.g. Matthews et al. 2010) targets (Kennedy et al. 2012a). This can also be applied to resolved sources when the source remains similar in scale to the beam full width at half-maximum.

2.1 Sample

We consider here a sample of 36 stars, 19 of which have planet detections from Johnson et al. (2007, 2008, 2010a,c, 2011a,b) and Bryan et al. (in preparation), 17 of which are control stars, that have been searched for planets as part of a survey using Lick and Keck observatories to search for planets orbiting 'retired' A stars (Johnson et al. 2006), but where nothing was detected.[2] All stars were observed in the RV programs such that the spectrum receives the same signal-to-noise ratio (S/N), regardless of stellar properties or sky conditions. Thus, the survey is complete to planets with velocity semi-amplitudes $K > 20\,\mathrm{m\,s^{-1}}$ and periods equal to the survey baseline of 6 yr (Johnson et al. 2010b). The non-detection limits equate approximately to an absence of planets on orbits shorter than 200 d, with a mass limit of around a Neptune mass at this semimajor axis, although the exact limits vary from target to target. The control sample were approximately matched to the planet sample in terms of distribution of stellar luminosity and distance. We only include stars within 160 pc of the Sun, of mass greater than $1.5\,M_{\odot}$ and $L > 15\,L_{\odot}$. This minimizes the probability of their lying outside the local bubble where interactions with the ISM can mimic debris disc emission (Kalas et al. 2002; Gáspár et al. 2008), as well as maximizes the probability of disc detection. The position of the sample on an HR diagram is shown in Fig. 1.

3 RESULTS

3.1 Photometry

In order to analyse the sample for emission from debris discs, it is first necessary to account for the stellar contribution to the emission. Optical and near-IR photometry is collected from numerous catalogues (Morel & Magnenat 1978; Mermilliod 1987; Moshir et al. 1993; Hauck & Mermilliod 1997; Perryman & ESA 1997; Høg et al. 2000; Cutri et al. 2003; Ishihara et al. 2010). These data were used to find the best-fitting stellar model, using the PHOENIX GAIA grid (Brott & Hauschildt 2005), via a χ^2 minimization, as in Kennedy et al. (2012a,b) and Wyatt et al. (2012). This method uses synthetic photometry over known bandpasses and has been validated against high S/N MIPS 24 μm data for DEBRIS targets, showing that the photospheric fluxes are accurate to a few per cent for main-sequence, AFG-type, stars.

Most stars in this sample are faint and have predicted photospheric fluxes lower than the PACS detection limit, thus any detected emission is likely to result from a debris disc, particularly at 160 μm.

[2] The two samples were originally the same size, but planets have recently been found orbiting one of the proposed control sample.

Table 1.

Object		ObsID	Date	$L_\star$ ($L_\odot$)	$M_\star$ ($M_\odot$)	$T_{\rm eff}$ (K)	Dist (pc)	Age (Gyr)	±	Phot 100 μm (mJy)	±	Phot 160 μm (mJy)	±	Obs100 μm (mJy)	±	Obs 160 μm (mJy)	±	χ_{100}	χ_{160}	Planet
HD 1100		1342223913/4	2011-07-11	17.9	1.53	4711	140.4	2.7	0.9	3.50	0.07	1.39	0.03	4.88	1.33	1.75	2.61	1.0	0.1	
HD 1502		1342225479/10	2011-07-24	12.4	1.61	4915	159.2	2.4	0.5	1.64	0.03	0.65	0.01	1.01	1.38	1.41	2.89	0.5	0.3	Y[7]
HD 4313		1342225497/8	2011-07-24	14.5	1.72	4939	137.0	2.1	0.4	2.46	0.04	0.98	0.02	0.28	1.40	0.00	2.82	1.5	0.3	Y[6]
HD 4917		1342225339/10	2011-07-23	11.9	1.72	4745	134.4	2.4	0.5	2.45	0.08	0.97	0.03	0.00	1.39	2.18	2.60	1.8	0.5	Y[9]
HD 7931		1342225330/1	2011-07-23	10.9	1.50	4780	124.1	3.2	0.8	2.67	0.04	1.06	0.02	2.04	1.33	0.00	2.61	0.5	0.4	
HD 12137		1342237470/1	2012-01-13	15.9	1.81	4896	137.2	1.8	0.4	3.00	0.04	1.19	0.02	4.59	1.34	0.00	2.66	1.2	0.4	
HD 18742		1342237830/1	2012-01-05	14.4	1.60	4933	135.3	2.3	0.5	2.54	0.05	1.01	0.02	0.00	1.43	3.02	2.89	1.8	0.7	Y[7]
HD 19659		1342237414/5	2012-01-12	11.6	1.59	5628	95.5	2.6	0.3	2.75	0.04	1.09	0.02	4.11	1.31	0.00	2.73	1.0	0.4	
HD 27536	V*EK Eri	1342241949/10	2012-03-20	12.7	1.67	5106	61.3	2.2	0.1	9.76	0.20	3.87	0.08	11.53	1.36	5.93	2.42	1.3	0.8	
HD 33240		1342242506/7	2012-03-28	14.4	1.70	4684	155.5	2.6	0.8	2.35	0.04	0.94	0.02	3.43	1.31	0.00	2.75	0.8	0.3	
HD 33844		1342242512/3	2012-03-28	13.4	1.75	4827	100.9	2.1	0.3	4.50	0.06	1.79	0.02	2.21	1.36	0.00	2.77	1.7	0.7	Y[9]
HD 34909		1342242530/1	2012-03-28	11.7	1.61	4942	132.8	2.5	0.4	2.124	0.04	0.84	0.02	<8.41	1.96	<46.43	9.27	3.0	4.9	
HD 39828		1342242664/5	2012-03-29	14.6	1.64	4839	127.4	2.4	0.5	3.06	0.05	1.22	0.02	1.19	1.20	0.00	2.83	1.5	0.4	
HD 72429	V*FK Cnc	1342230053/4	2011-10-03	11.1	1.59	5753	140.1	2.7	0.3	1.15	0.02	0.45	0.01	3.39	1.44	9.02	3.21	1.6	2.7	
HD 83752		1342232210/1	2011-11-10	10.6	1.56	5990	115.7	2.7	0.2	1.42	0.03	0.56	0.01	12.68	1.57	22.07	3.73	7.5	5.8	
HD 88737	HR 4012	1342221944/5	2011-06-01	10.4	1.60	6094	56.8	2.6	0.2	5.50	0.08	2.18	0.03	3.47	1.40	0.00	2.86	1.4	0.8	
HD 90043	*24 Sex	1342223308/9	2011-06-29	16.3	1.54	4971	77.5	2.7	0.4	8.49	0.16	3.37	0.06	8.66	1.43	3.42	2.76	0.1	<0.1	Y[5]
HD 95089		1342223464/5	2011-06-22	14.0	1.60	4861	139.1	2.5	0.6	2.44	0.05	0.97	0.02	4.04	1.31	4.97	2.63	1.2	1.5	Y[6]
HD 102956		1342221826/7	2011-05-29	11.8	1.68	4971	126.3	2.3	0.5	2.32	0.03	0.92	0.01	2.13	1.38	3.61	2.84	0.1	0.9	Y[2]
HD 108863		1342223898/9	2011-07-10	17.0	1.85	4837	139.3	1.8	0.4	2.98	0.05	1.18	0.02	4.35	1.40	3.05	3.09	1.0	0.6	Y[7]
HD 116029		1342233220/1	2011-11-27	11.7	1.58	4846	123.2	2.7	0.5	2.61	0.05	1.04	0.02	2.56	1.35	0.00	2.57	0.0	0.4	Y[7]
HD 118082		1342237222/3	2012-01-12	14.0	1.57	4814	144.1	2.7	0.6	2.36	0.06	0.94	0.02	1.69	1.33	5.49	3.06	0.5	1.5	
HD 125607		1342224634/5	2011-07-21	10.6	1.52	4964	133.0	2.8	0.6	1.88	0.03	0.75	0.01	2.05	1.38	0.00	2.63	0.1	0.3	
HD 131496		1342235118/9	2011-12-24	10.1	1.61	4803	110.0	2.7	0.5	2.90	0.04	1.15	0.02	7.56	1.43	5.70	3.00	3.4	1.5	Y[7]
HD 142091	κ CrB	1342234353/4	2011-12-15	12.0	1.72	4866	30.5	2.2	0.1	43.52	0.72	17.36	0.29	334.85	17.38	192.33	11.02	17.2	16.4	Y[1]
HD 142245		1342225421/2	2011-07-24	13.8	1.69	4816	109.5	2.3	0.3	4.04	0.06	1.60	0.02	2.62	1.39	2.66	3.08	1.0	0.3	Y[7]
HD 158038		1342229965/6	2011-10-01	11.9	1.65	4911	103.6	2.5	0.3	3.62	0.07	1.45	0.03	3.52	1.51	0.00	2.53	0.1	0.6	Y[7]
HD 166494		1342221813/4	2011-05-28	9.9	1.53	5594	114.7	3.0	0.3	1.66	0.06	0.66	0.02	0.00	1.29	0.67	3.47	1.3	<0.1	
HD 167042	LTT 15382	1342234341/2	2011-12-15	10.6	1.51	4978	50.2	2.9	0.4	13.07	0.23	5.19	0.09	12.12	1.44	2.71	2.76	0.6	0.9	Y[4]
HD 180053		1342234072/3	2011-12-14	10.5	1.70	5104	126.3	2.3	0.2	1.91	0.10	0.76	0.04	1.63	1.53	0.00	4.17	0.2	0.2	Y[9]
HD 181342		1342216480/1	2011-03-20	12.4	1.75	4876	110.6	2.1	0.3	3.39	0.05	1.35	0.02	3.46	1.43	0.00	3.20	<0.1	0.4	Y[6]
HD 184010	HR 7421	1342243724/5	2012-04-05	16.4	1.60	5004	60.5	2.3	0.3	13.80	0.25	5.47	0.10	10.80	1.56	10.14	4.07	1.9	1.2	
HD 188386		1342231682/3	2011-10-30	12.4	1.55	4821	143.5	2.7	0.7	2.16	0.04	0.86	0.02	3.40	1.37	0.00	3.30	0.9	0.3	C[10]
HD 208585		1342220939/10	2011-05-14	14.6	1.52	4870	145.3	2.7	0.8	2.37	0.05	0.94	0.02	14.50	1.70	11.19	3.60	7.5	2.9	
HD 210702	HR 8461	1342235309/10	2011-12-25	13.2	1.65	4969	54.9	2.3	0.3	13.68	0.29	5.43	0.12	82.30	4.27	44.51	2.55	15.9	15.4	Y[3]
HD 220952		1342234094/5	2011-12-14	12.0	1.50	4905	125.2	2.9	0.5	2.50	0.05	0.99	0.02	1.59	1.39	2.69	2.94	0.6	0.6	

[1]Johnson et al. (2008), [2]Johnson et al. (2010c), [3]Johnson et al. (2007), [4]Johnson et al. (2008), [5]Johnson et al. (2011a), [6]Johnson et al. (2010a), [7]Johnson et al. (2011b), [9]Bryan et al. (in preparation), [10] Johnson (private communication).

Details of our sample taken from the SPOCSIV catalogue, predicted photospheric fluxes calculated using the best-fitting stellar model (Brott & Hauschildt 2005) and the *Herschel* observed fluxes. The stellar properties were determined from fitting isochrones to the spectroscopic properties of the stars, using the stellar models of Girardi et al. (2002). The ages were determined from interpolating the spectroscopic properties on to the Yonsei–Yale model evolution grids, as described in Valenti & Fischer (2005). C refers to planet candidates that are still awaiting confirmation.

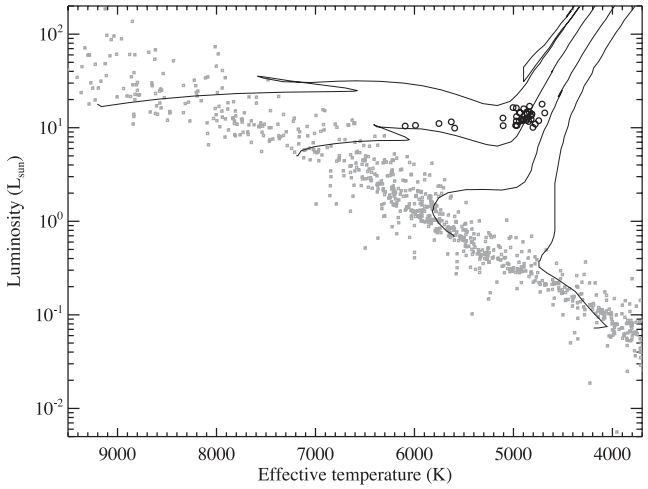

Figure 1. Our sample plotted on an HR diagram (large black circles), alongside stars from the UNS sample (small grey dots), an unbiased sample of nearby main-sequence stars (Phillips et al. 2010) and stellar evolution tracks taken from Girardi et al. (2002) for 0.6, 1, 1.5 and 2.0 $M_{\odot}$. Tracks start at the zero-age main sequence and move to the upper right over time. Our sample of subgiants have similar luminosities to main-sequence A stars, but are cooler.

However, emission from background objects may contribute significantly to emission in the far-IR and sub-mm and without the stellar emission to guide the pointing, we are reliant on *Herschel's* pointing to indicate the location of the star, which on average is accurate to within 1.32 arcsec in our observations.[3] There is clear evidence that some previous *Herschel* observations of debris discs have been contaminated by emission from background objects (e.g. Donaldson et al. 2012), particularly at 160 μm, although this is only found to be important for 1 or 2 of our sample (see Section 3.3).

Flux densities for each source are measured by fitting a model PSF (observations of Alpha Boo reduced in the same way as the data) at the supposed source location in each image. For non-detections an attempt to make a similar fit is made, but the measured flux is lower than the measured noise. For the sources where the emission was resolved, we do aperture photometry and use a sufficiently large aperture that all disc emission is captured. We assume that the emission is centred on the *Herschel* pointing, unless sufficient emission is detected to suggest that the centre is offset from the pointing, in which case the centring is adjusted appropriately. Uncertainties were calculated using the results from the least-squares PSF fitting, and were checked for consistency against the standard deviation of a large number of apertures of sizes 5 and 8 arcsec (the sizes for optimal S/N at 100 and 160 μm) and placed randomly near the map centres. These integrated fluxes and uncertainties were compared to predictions for the stellar photosphere, as shown in Fig. 2.

Fig. 2 shows that for the majority of sources, the predicted photospheric flux is too low to have been detected in the *Herschel* observations. A significant detection of the source (excess and/or photosphere) was detected for a total of 15 (5) sources at 100 μm (160 μm), shown by the blue crosses. Significant emission, 3σ above the stellar photosphere, shown by the red crosses, was detected for six sources at 100 μm, namely κ CrB (HD 142091), HR

[3] A weighted average of the absolute pointing error for obsID 1342216480-1342221945 = 2.36 arcsec, 1342223464-1342225498 = 1.45 arcsec, 1342229965-1342237471 = 1.1 arcsec, 1342241949-1342243725 = 0.8 arcsec.

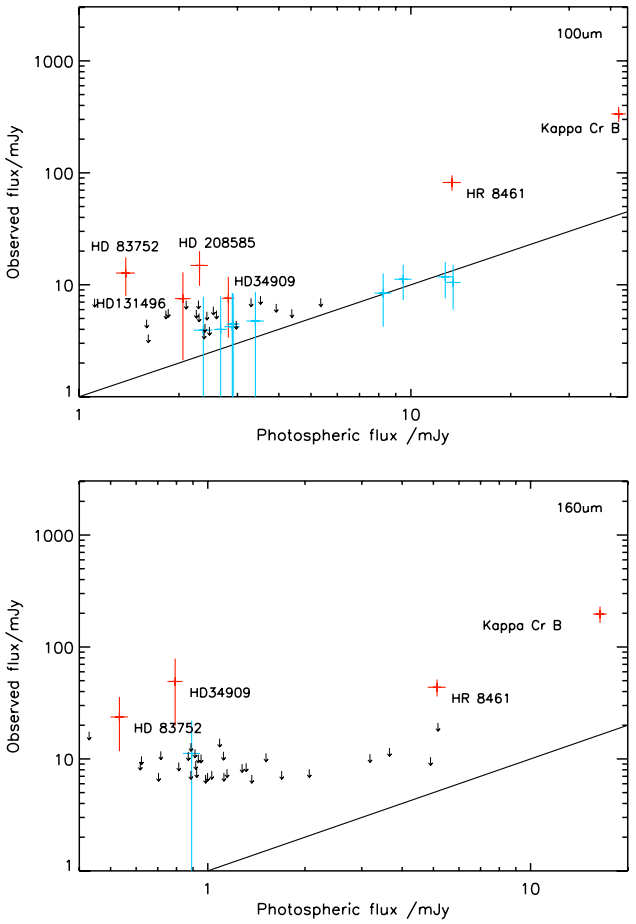

Figure 2. The photospheric flux, predicted using stellar models (as discussed in Section 3.1) compared to the observed flux at 100 μm (top) and 160 μm (bottom). The red points show 3σ detections of an excess, the blue points, 3σ detections of the system, both with 3σ error bars, and the black arrows the 3σ upper limits on the observed flux, when the detection is below 3σ.

8461 (HD 210702), HD 34909, HD 83752, HD 208585 and HD 13496, but only four at 160 μm,κ CrB (HD 142091), HR 8461 (HD 210702), HD 34909 and HD 83752.

For each of our detections, the offset of the peak from the nominal stellar position was also determined. These are shown in Fig. 3, compared to the pointing accuracy of *Herschel*. All detected sources have small offsets from the nominal *Herschel* pointing (close to or less than the 1σ error), apart from HD 83752, suspected of being contaminated with background emission, as described below. HD 34909 has not been included is in this plot as the emission is not consistent with a point source (see later discussion).

For the sources where the emission was consistent with originating in a debris disc, we used the spectral energy distribution (SED) to obtain an estimate of the disc temperature. In order to determine this, we make the simplest possible assumption; that the dust grains emit like blackbodies. The inefficient emission properties of real grains will reduce the flux at long wavelengths. In order to better model this, we have introduced the free parameters λ_0 and β and reduced the blackbody flux by a factor of $(\frac{\lambda}{\lambda_0})^{-\beta}$ at wavelengths longer than λ_0. λ_0 and β are very poorly constrained, but nonetheless illustrative of the reduced emission anticipated at long wavelengths, that could be relevant for future observations, for example with ALMA.

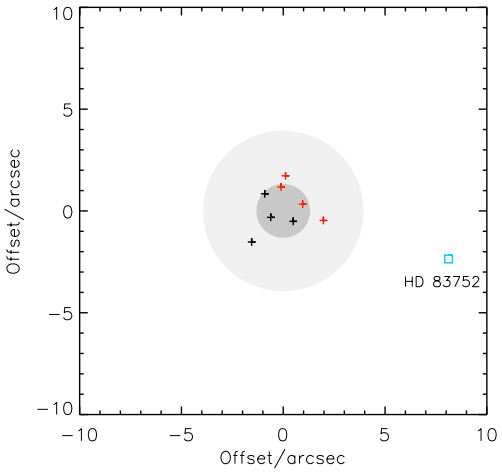

Figure 3. The offset of the centre of the observed emission at 100 μm, compared to the nominal location of the star. The grey circles show the weighted average absolute pointing error of our *Herschel* observations, 1.3 arcsec at 1σ and 3.9 arcsec at 3σ. The black points show the debris detections (κ CrB, HR 8461, HD 208585 and HD 13496), whilst the red points, show the stars for whom the emission at 100 μm was greater than 3σ above the error on the observations. The blue square shows HD 83752, whose excess emission is suspected of being contaminated with background emission. The emission surrounding HD 34909 is not point-like and, therefore, omitted from this plot.

3.2 Notes on the six sources where an IR excess was detected

3.2.1 Kappa Cr B

This is the strongest detection in our sample. The debris disc is resolved at both 100 and 160 μm, and we refer the reader to Bonsor et al. (2013) for detailed modelling of this source. Fig. 4 shows an SED including observations of this source at all wavelengths and a blackbody fit to the disc emission. RV observations of κ CrB

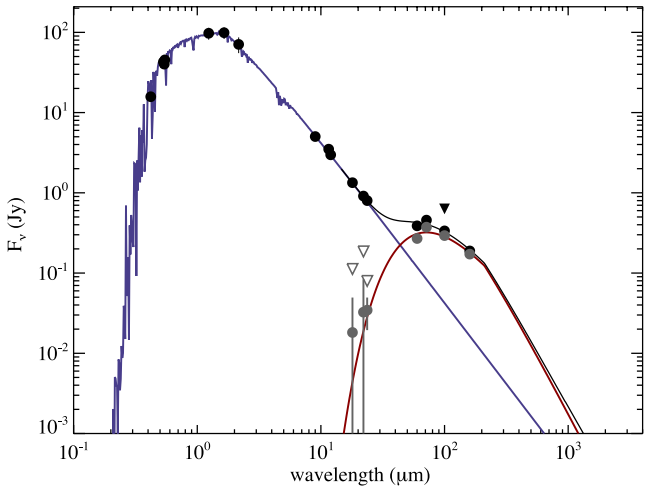

Figure 4. SED for κ CrB (Bonsor et al. 2013). Photometry is shown as black dots or black triangles for upper limits. Disc (i.e. photosphere-subtracted) fluxes and upper limits are shown as grey dots and open triangles. The stellar spectrum is shown as a blue line and the red line shows a blackbody fit to the disc emission, modified at long wavelengths to illustrate the decrease in emission of more realistic grains. The disc has a blackbody temperature of 72 ± 3 K, which corresponds to a blackbody radius of 53 ± 5 au. This is subtly different from Bonsor et al. (2013), where λ_0 and β were free parameters.

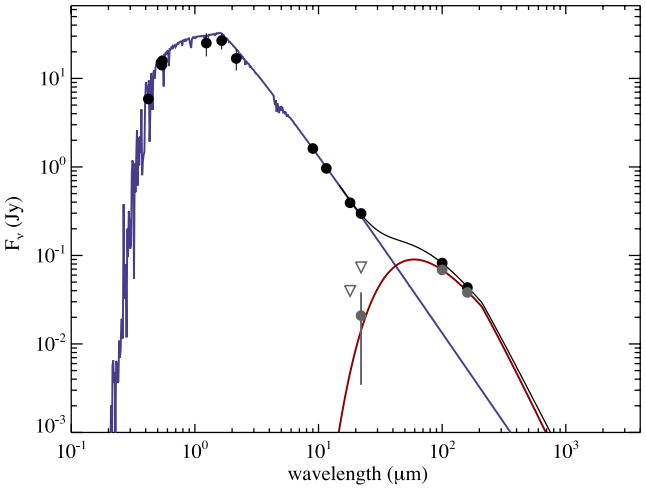

Figure 5. SED of HR 8461, plotted in the same manner as Fig. 4, including a *WISE* measurement at 24 μm. The disc has a blackbody temperature of 86 ± 11 K, which corresponds to a blackbody radius of 38 ± 10 au.

find evidence for two companions, a close-in, $m\sin I = 2.1\,M_J$, on a mildly eccentric ($e = 0.125 \pm 0.049$) orbit, with a semimajor axis of 2.8 ± 0.1 au (Johnson et al. 2008) and a second companion, deduced from a trend found in the long-term RV monitoring of this source. AO imaging failed to detect this second companion, thus, if it is on a circular orbit, its semimajor axis lies interior to 70 au (see Bonsor et al. 2013 for full details). Modelling of the resolved images combined with the SED information shows that the dusty material is either found in a single wide dust belt, stretching from 20 to 220 au, or two narrow thin dust belts centred on 40 and 165 au.

3.2.2 HR 8461

RV monitoring found a planet with $M\sin I = 2.0\,M_J$ in a 341.1 d orbit around HR 8461 (Johnson et al. 2007). As can be seen in Fig. 2, the emission is clearly significantly above the predicted stellar photosphere at both 100 μm (16σ) and 160 μm (15σ). The *Herschel* data points are plotted alongside the stellar spectrum in Fig. 5. A blackbody fit to the data yields a blackbody temperature of 86 ± 11 K, which would correspond to a disc radius of 37.9 ± 9.7 au if the dust acts like a blackbody. Fig. 6 shows the *Herschel* images of this source at both 100 and 160 μm. The disc is marginally resolved at 100 μm, as shown by star-subtracted image in the bottom panel of Fig. 6. Fitting a simple ring to the image finds a disc radius of roughly 130 au, somewhat larger than the blackbody radius, but not inconsistent with models that suggest that grains with realistic emission properties can be significantly hotter than blackbodies (Bonsor & Wyatt 2010; Kains, Wyatt & Greaves 2011; Booth et al. 2013). The position angle and inclination of the disc in this fit are poorly constrained.

3.2.3 HD 208585

A 100 μm excess is clearly detected (7.1σ) for HD 208585, and a marginal excess at 160 μm, with a significance of 2.8σ. The emission is not resolved at either wavelength. In Fig. 7, we plot the *Herschel* data points, alongside the full stellar spectrum. The temperature is poorly constrained due to the marginal detection at 160 μm; the blackbody fit yields 56 K with a 3σ range of 25–120 K. The wide range of disc temperatures, and the fact that the disc temperature and normalization are correlated, mean that the

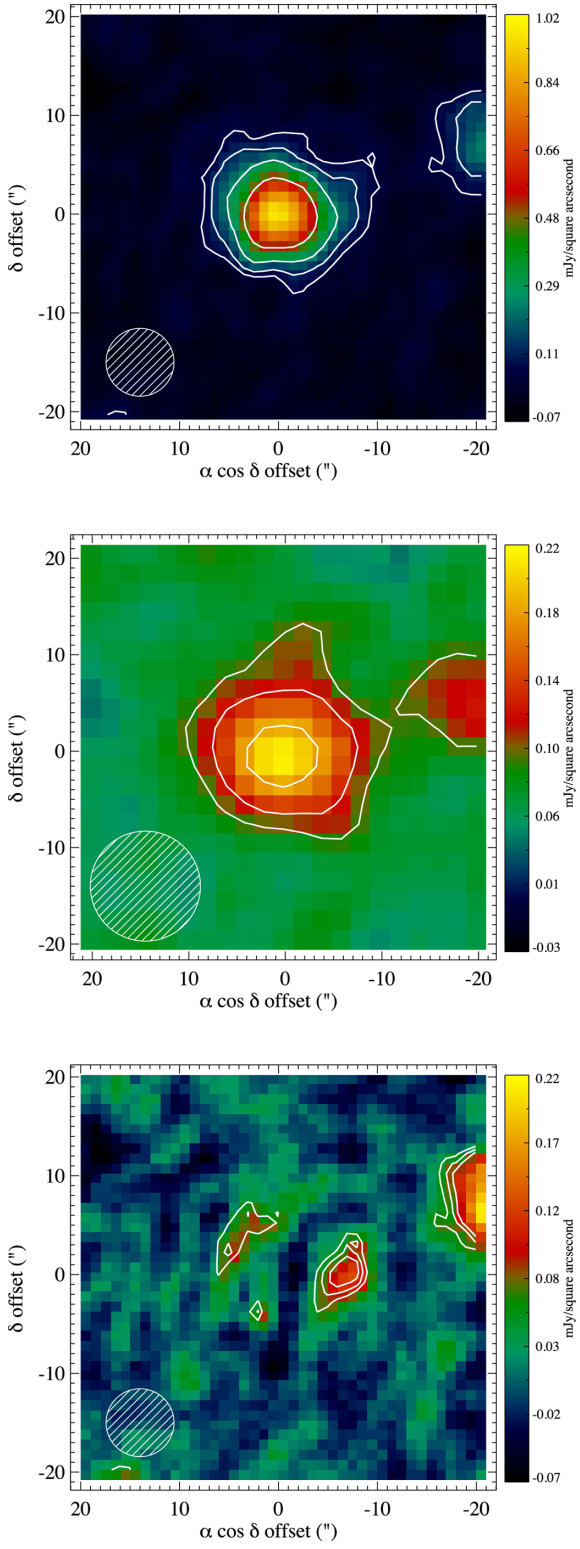

Figure 6. The *Herschel* images of HR 8461 at 100 μm (top) and 160 μm (middle), with contours showing detection levels of 3σ, 6σ, 12σ, where $\sigma = 2.09 \times 10^{-5}$ at 100 μm and $\sigma = 5.7 \times 10^{-5}$ at 160 μm. The bottom panel plots the residuals after subtracting a stellar PSF scaled to the peak, with contours at $3\sigma, 4\sigma, 5\sigma$. This shows that the disc is marginally resolved at 100 μm. A similar plot shows that it is not resolved at 160 μm.

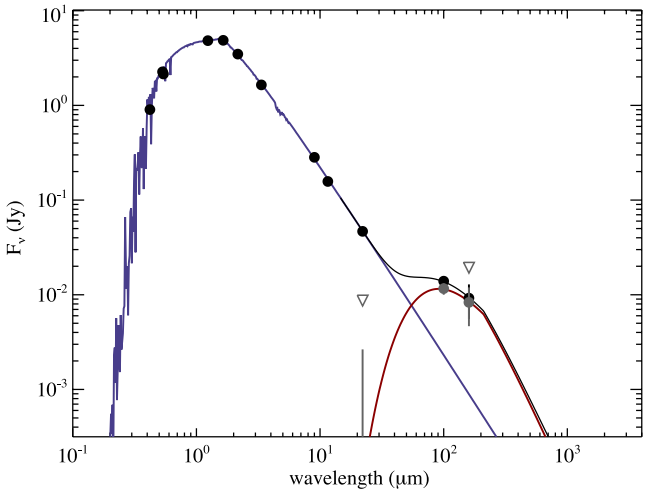

Figure 7. SED of HD 208585, plotted in the same manner as Fig. 4. The disc emission is not well constrained, but we fit a blackbody temperature of 56^{+65}_{-30} K, which corresponds to a blackbody radius of 94^{+440}_{-20} au.

uncertainties are asymmetric about 56 K. They were estimated using a grid in temperature versus normalization space that calculates the deviation from the best-fitting χ^2 at each point.

This source has been searched for RV companions, with a total of 11 RV measurements, over a time period spanning 5 yr, but currently there have been no detections of any companions.

3.2.4 HD 131496

A 2.2 M_J planet was detected orbiting HD 131496 by Johnson et al. (2011b). Excess emission was found at this source at a level of 3.4σ at 100 μm, but not detected at 160 μm (1.5σ excess). As for HD 208585, the disc temperature is not well constrained, with a best fit of 42 K and a 3σ range of 10–370 K. Fig. 8 shows the SED for HD 131496.

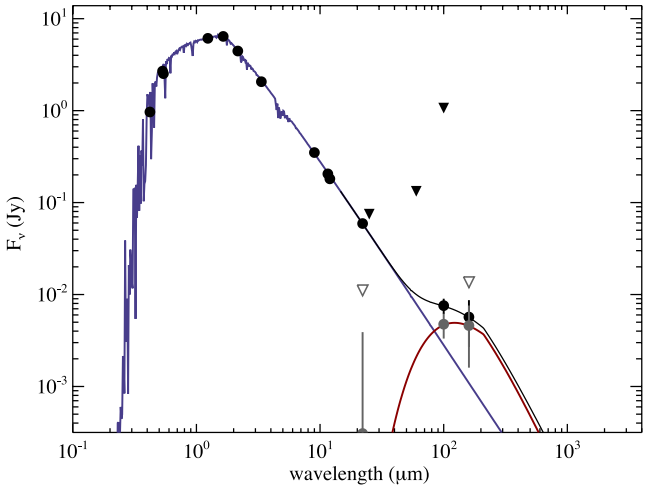

Figure 8. SED of HD 131496, plotted in the same manner as Fig. 4, but with only a single data point the disc temperature is poorly constrained.

3.2.5 HD 83752

The emission observed close to this object is likely to be from a background source. The predicted stellar photosphere is significantly below the *Herschel* detection limits at both wavelengths and the emission detected in the field of view of this object is offset from the nominal stellar position by 8.5 arcsec, larger than the 3.1 arcsec, 3σ absolute pointing error of the *Herschel* observations for this target, as can be seen in Fig. 3. In addition to this, the observed emission increases from 100 to 160 μm, by a factor of 2, a feature generally reminiscent of the emission from cold, distant galaxies. The best-fitting blackbody temperature would need to be less than 30 K, equivalent to blackbody grains situated further than 350 au from this 10.7 $L_{\odot}$ star. Although there have been previous detections of cold debris discs with *Herschel* (Krivov et al. 2013), in this case a diameter of 700 au corresponds to 6 arcsec at 116 pc, and if this really were a debris disc of blackbody size or larger, it would appear extended in our *Herschel* observations, assuming that the dusty material is not found in a clump at this radial distance. We, therefore, conclude that this emission likely originates in a background galaxy, not a debris disc orbiting HD 83752.

3.2.6 HD 34909

The *Herschel* image (Fig. 9) of this source reveals extended emission filling a significant proportion of the field of view at both 100 and 160 μm. HD 34909 is situated in a very dusty region of the sky, at 23° from the galactic plane, close to a star-forming region in Orion. The emission observed is likely to result from dust in this molecular cloud and it is very difficult to assess whether there is additional emission from the subgiant, or a potential debris disc orbiting HD 34909. We place an upper limit on the flux from a disc that could be hidden in this system (see Table 1).

3.3 Background galaxy contamination in our sample

Contamination of observations at the *Herschel* wavelengths by background sources is common. The level of such contamination in PACS data is characterized by Sibthorpe et al. (2013). The contamination in our observations can be assessed in comparison with such results. If we consider the weighted average 3σ absolute pointing error of *Herschel* PACS in our observations of 3.94 arcsec and the average 3σ error on our observations of ±5.7 mJy at 100 μm, according to the results of Sibthorpe et al. (2013), there is a 1.5 per cent chance of confusion by one or more background sources. Given that we have observed 36 stars, this means that the probability of no stars being contaminated is 58 per cent, whilst the probability of one star being contaminated by a background detection is 31.8 per cent and of two stars being contaminated is 4.8 per cent. This is critically important in our assessment of our detection statistics as it means that the chances of one of our detections resulting from a background object is not insignificant (31.8 per cent), although there is only a slim chance of more than one of our detections being contaminated in this manner (4.8 per cent). We should, however, note that for some of our detections there is good evidence to suggest that we are observing debris discs rather than galaxies, for example, the extended nature of κ CrB and HR 8761.

We note that both HD 83752 and HD 34909 should be excluded from the above analysis. HD 34909 is a separate case as it is located in a region of the sky known to be contaminated by the dusty emission from star formation. HD 83752 has an offset of 8.5 arcsec from the nominal *Herschel* pointing, more than 3σ from the nominal *Herschel* pointing. There is a 96 per cent chance of one of our stars having a detectable background source within 10 arcsec of the *Herschel* pointing for our stars. Thus, our detection of emission close to HD 83752 is consistent with our statistical analysis.

3.4 Summary

Excess emission, consistent with a debris disc, was found for 4/36 (2/36) of the subgiants in our sample, namelyκ CrB, HR 8461, HD 208585 and HD 131496 (κ CrB and HR 8461) at 100 μm (160 μm). Three of the detections are planet-hosting stars (κ CrB, HR 8461 and HD 131496), whilst HD 208585 has no current planet detections. This leaves us with 3/19 planet hosts that have debris and 1/17 control (non-planet host) stars with debris.

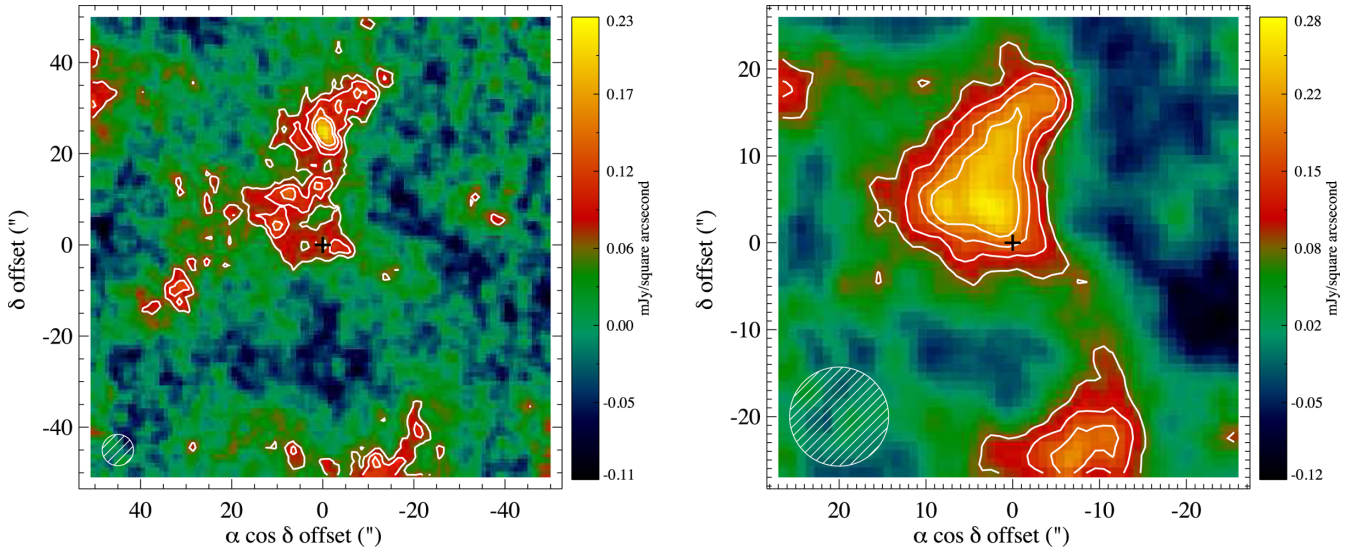

Figure 9. The *Herschel* images of HD 34909 at 100 (left) and 160 μm (right) showing clear contamination from the dusty, star-forming region at a similar location on the sky. The cross shows the nominal location of the star and the contours show 2σ, 3σ, 4σ, 5σ detection levels, where $\sigma = 2.9 \times 10^{-5}$ at 100 μm and $\sigma = 1.7 \times 10^{-4}$ at 160 μm.

4 COMPARISON WITH OBSERVATIONS OF DEBRIS DISCS ORBITING MAIN-SEQUENCE STARS

Our four debris disc detections for subgiants provide a tiny sample compared to the wealth of observations already obtained for main-sequence stars. It is, nonetheless, interesting to assess whether our sample shows similar trends to those observed in the population of debris discs orbiting main-sequence stars. A prime example being the decrease in brightness of the discs with age of the star. Subgiants, being older than their main-sequence counterparts (at least for similar mass stars), provide crucial information regarding the continuation of this trend to later times.

A simple toy model developed in Wyatt et al. (2007b, c) provides a reasonable description of the time evolution of the disc luminosity, by considering each disc to have a flat, then 1/age dependence, which is a reasonable approximation to models that consider the evolution of the size distribution in more detail (e.g. Löhne, Krivov & Rodmann 2008; Gáspár, Rieke & Balog 2013). This fits the observational data for both debris discs orbiting main-sequence A stars (Wyatt et al. 2007c) and FGK stars (Kains et al. 2011). Here, we compute a model population, based on the work of Wyatt et al. (2007c), but applied to the specific properties, e.g. age, luminosity and distance, of our sample of subgiants. This model, therefore, takes into account any differences between our subgiants and main-sequence stars, including evolution in luminosity or the effects of radiation pressure that remove the smallest grains in the disc. Initially, we focus on the fate of debris discs observed around main-sequence A stars, using the model parameters derived in Wyatt et al. (2007c), as isochrone fitting using the stellar models of Girardi et al. (2002) suggests that our subgiants evolved from similar mass stars (Johnson et al. 2007, 2008, 2010a,c, 2011a,b).

This model population is plotted in terms of its fractional luminosity and temperature in Fig. 10. The detections from our observations are shown (circles) for comparison. The top axis shows the equivalent blackbody temperature for a disc orbiting a 15 $L_\odot$ star for reference, although, we point out here that the real radii of detected discs may differ from their blackbody radii. This model population shows a clear upper limit in fractional luminosity as a function of temperature (or radius), with no discs inhabiting the top-right corner of this plot. As collisions grind down the material in the debris discs, with faster evolution for closer in discs, there is a maximum mass that can survive in steady state as a function of time and disc radius. The similar ages of our stars (see Table 1) means that this maximum mass, which translates into a maximum fractional luminosity, is predominantly a function of the disc radius, and can be clearly seen in the upper envelope of the model population on Fig. 10. Two of our detections (κ CrB and HR 8461) lie above this maximum. This does not mean that these discs need be unphysically massive, since the model population is derived with the parameters of an average disc, whereas some discs would be expected to have maximum disc masses that can lie an order of magnitude above that of the average disc, and it is such discs that would be most easily detected. However, an alternative explanation could be that some individual sources do not fit within the context of this simple model. Notably, the resolved images of κ CrB indicate that the emission results from either a wide belt, or two distinct belts (Bonsor et al. 2013), whereas the model assumed all discs to be described by a single narrow ring.

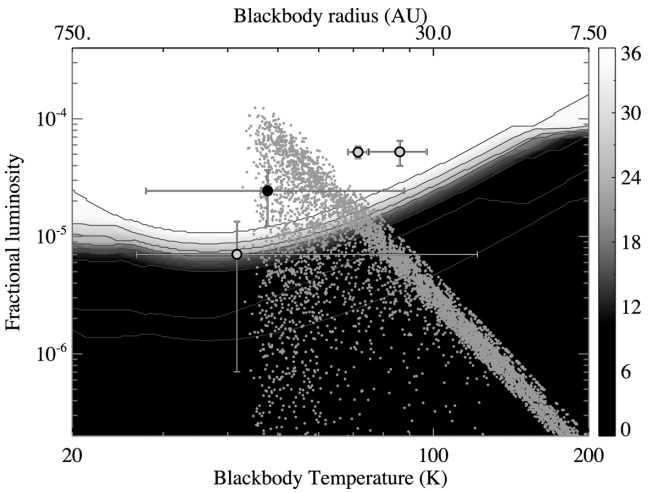

Figure 10. The cumulative detection limits for discs orbiting all of the stars in our sample, as a function of the disc blackbody temperature and fractional luminosity (ratio of the total disc luminosity to the total stellar luminosity), with 1σ error bars. The equivalent blackbody radius for a disc orbiting a 15 $L_\odot$ star is plotted on the top axis for reference. The discs that were detected in our sample are plotted by the large circles, empty circles for the planet-hosts and filled circles for the non-planet hosts, whilst the small circles show the model population, as described in Section 4. It should be noted that there is an artificial upper (lower) limit in radius (blackbody temperature), which is imposed by the model population based on the work of Wyatt et al. (2007c).

Only a small fraction of the model population could have been detected, due to the limited sensitivity of our observations. We characterized this, by calculating whether a simple, thin, blackbody disc at each temperature, with each fractional luminosity, would have been detected orbiting each star in our survey. The grey lines on Fig. 10 show the fraction of this model population that would have been detected in our *Herschel* observations. The white (black) shaded area shows the parameter space where debris discs would have been detected around all (no) stars in our survey. In order to compare the model population with our observations, we calculate the detection rate that would be obtained if this model population were observed with *Herschel* and the observation limits of our survey. This is done by assigning each star a disc from the model population and comparing the emission from the disc to the sensitivity of the *Herschel* observations obtained for that source, thus determining whether or not the disc would have been detected. We note here that are survey detects debris discs more readily around nearby stars. Repetition of this process leads to a range of detection rates, as shown in Fig. 11. The mean detection rate obtained is 7/36 (3.4/36) at 100 (160) μm, which is higher than the detection rates found in our observations of 4/36 (2/36). However, further analysis finds that the probability of detecting only 4/36(2/36) debris discs, given this distribution is within 2σ (1σ) of the mean detection rate at 100 μm (160 μm). In other words, our detection rate is on the low side, but not inconsistent with being derived from the model population.

Although not required to explain the observations, one potential issue with the comparison between the model population and our observations should be noted here. The model of Fig. 10 for the debris discs orbiting our subgiants assumed that these are descended from a main-sequence population with disc parameters (e.g. planetesimal strength, size and orbital eccentricities) that were optimized to explain observations of the evolution of debris discs around main-sequence A stars (Rieke et al. 2005; Su et al. 2006; Wyatt et al. 2007c), with spectral types B8V to A9V. However, the disc parameters required to explain the population of main-sequence discs around Sun-like stars is different (Kains et al. 2011), as is the

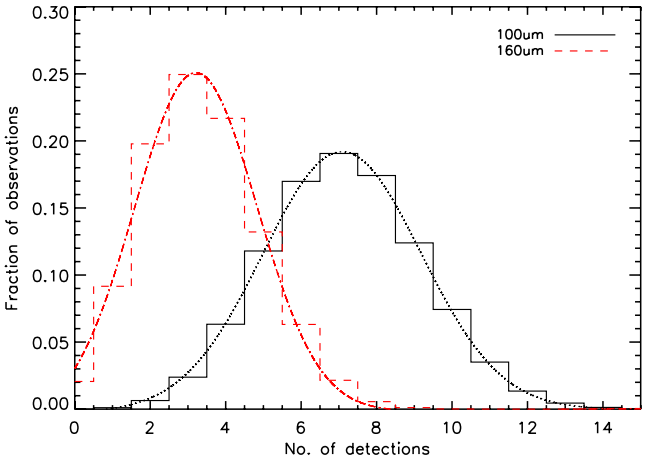

Figure 11. A histogram to show the number of detections found after repeated observations of the model population at 100 μm (black solid line) and 160 μm (red dashed line). The mean detection rate was found to be 7/36 at 100 μm and 3.4/36 at 160 μm. A Gaussian was fitted to distribution, with width $\sigma = 2$ (100 μm, black dotted line) and $\sigma = 1.6$ (160 μm, red dash–dotted line).

main-sequence lifetime. Thus, if our stars evolved from a different distribution of spectral types on the main sequence, our predicted detection statistics could vary significantly. This detail is particularly relevant given the current discussion in the literature regarding the masses of planet-hosting subgiants, including those used in this survey (Lloyd 2011, 2013; Schlaufman & Winn 2013). Had the rate we observed been significantly different to that predicted from the model, this could have been interpreted in terms of the properties of the main sequence progenitors. As it is, there is no evidence to exclude these subgiants' discs being evolved versions of the population seen around main-sequence A stars, particularly when it is noted that additional factors, such as dynamical instabilities, tend to reduce the fraction of stars with detectable debris around older stars.

To summarize, our observations do not currently provide any evidence against a very simple model for the collisional evolution of debris discs from the main sequence to the subgiant branch, nor do they provide further evidence regarding the main-sequence origin of our subgiant sample. As further detections of debris discs orbiting subgiants are obtained this analysis can be extended and the new data used to repeat the analysis of Wyatt et al. (2007c) or Kains et al. (2011) including a further time bin for stars on the subgiant branch, thus further constraining our understanding of the collisional evolution of debris discs.

5 CONCLUSIONS

We have observed 36 subgiants with *Herschel* PACS at 100 and 160 μm to search for the presence of excess emission from debris discs. All our stars have been searched for the presence of RV companions as part of the Johnson et al. program at the Keck/Lick observatories, with close-in, planetary companions detected for 20/36 stars. We detected excess emission, thought to be from debris discs, around 4/36 (2/36) of our sample at 100 μm (160 μm). Observations at *Herschel* wavelengths are frequently contaminated by emission from background galaxies. Whilst we acknowledge that there is a 30 per cent chance of emission from a background galaxy around one of our sources mimicking a debris disc (Sibthorpe et al. 2013), we note that there is a <5 per cent chance of contamination for more than one of our stars. Our detections form 3/19 of the planet-host sample and 1/17 of the control sample. Such a small number of detections provide no evidence that the detection rate for debris discs around stars with planets is different to that around stars without planets. These observations provide an important constraint for debris disc models, informing us of the fraction of stars with detectable discs at the end of the main sequence, which should be included in future models of debris disc evolution. These detections illustrate that large quantities of dusty material can survive the star's main-sequence evolution, providing a potential link with observations of pollution and dust around white dwarfs.

ACKNOWLEDGEMENTS

AB acknowledges the support of the ANR-2010 BLAN-0505-01 (EXOZODI). MCW and GK acknowledge the support of the European Union through ERC grant number 279973. We thank Marta Bryan for useful discussions that improved the quality of this manuscript.

REFERENCES

Augereau J.-C., Beust H., 2006, A&A, 455, 987
Augereau J. C., Nelson R. P., Lagrange A. M., Papaloizou J. C. B., Mouillet D., 2001, A&A, 370, 447
Barber S. D., Patterson A. J., Kilic M., Leggett S. K., Dufour P., Bloom J. S., Starr D. L., 2012, ApJ, 760, 26
Beichman C. A. et al., 2006, ApJ, 652, 1674
Bonsor A., Wyatt M., 2010, MNRAS, 409, 1631
Bonsor A., Mustill A. J., Wyatt M. C., 2011, MNRAS, 414, 930
Bonsor A., Kennedy G. M., Crepp J. R., Johnson J. A., Wyatt M. C., Sibthorpe B., Su K. Y. L., 2013, MNRAS, 431, 3025
Booth M. et al., 2013, MNRAS, 428, 1263
Bowler B. P. et al., 2010, ApJ, 709, 396
Brott I., Hauschildt P. H., 2005, in Perryman M. A. C., Turon C., O'Flaherty K. S., eds, ESA SP-576: A PHOENIX Model Atmosphere Grid for Gaia. ESA, Noordwijk, p. 565
Bryden G. et al., 2006, ApJ, 636, 1098
Bryden G. et al., 2009, ApJ, 705, 1226
Chiang E., Kite E., Kalas P., Graham J. R., Clampin M., 2009, ApJ, 693, 734
Churcher L., Wyatt M., Smith R., 2011a, MNRAS, 410, 2
Churcher L. J. et al., 2011b, MNRAS, 417, 1715
Currie T., Plavchan P., Kenyon S. J., 2008, ApJ, 688, 597
Cutri R. M. et al., 2003, VizieR Online Data Catalog, 2246, 0
Debes J. H., Sigurdsson S., 2002, ApJ, 572, 556
Debes J. H., Walsh K. J., Stark C., 2012, ApJ, 747, 148
Donaldson J. K. et al., 2012, ApJ, 753, 147
Farihi J., Jura M., Zuckerman B., 2009, ApJ, 694, 805
Fruchter A. S., Hook R. N., 2002, PASP, 114, 144
Galland F., Lagrange A., Udry S., Chelli A., Pepe F., Queloz D., Beuzit J., Mayor M., 2005, A&A, 443, 337
Gänsicke B. T., Marsh T. R., Southworth J., Rebassa-Mansergas A., 2006, Science, 314, 1908
Gänsicke B. T., Marsh T. R., Southworth J., 2007, MNRAS, 380, L35
Gänsicke B. T., Koester D., Farihi J., Girven J., Parsons S. G., Breedt E., 2012, MNRAS, 424, 333
Gáspár A., Rieke G. H., Balog Z., 2013, ApJ, 768, 25
Gáspár A., Su K. Y. L., Rieke G. H., Balog Z., Kamp I., Martínez-Galarza J. R., Stapelfeldt K., 2008, ApJ, 672, 974
Girardi L., Bertelli G., Bressan A., Chiosi C., Groenewegen M. A. T., Marigo P., Salasnich B., Weiss A., 2002, A&A, 391, 195
Greaves J. S., Wyatt M. C., Bryden G., 2009, MNRAS, 397, 757
Hauck B., Mermilliod M., 1997, VizieR Online Data Catalog, 2215, 0
Hillenbrand L. A. et al., 2008, ApJ, 677, 630
Høg E. et al., 2000, A&A, 355, L27

Holland W. S. et al., 1998, Nature, 392, 788
Ishihara D. et al., 2010, A&A, 514, A1
Johnson J. A., Marcy G. W., Fischer D. A., Henry G. W., Wright J. T., Isaacson H., McCarthy C., 2006, ApJ, 652, 1724
Johnson J. A. et al., 2007, ApJ, 665, 785
Johnson J. A., Marcy G. W., Fischer D. A., Wright J. T., Reffert S., Kregenow J. M., Williams P. K. G., Peek K. M. G., 2008, ApJ, 675, 784
Johnson J. A., Howard A. W., Bowler B. P., Henry G. W., Marcy G. W., Wright J. T., Fischer D. A., Isaacson H., 2010a, PASP, 122, 701
Johnson J. A., Aller K. M., Howard A. W., Crepp J. R., 2010b, PASP, 122, 905
Johnson J. A. et al., 2010c, ApJ, 721, L153
Johnson J. A. et al., 2011a, AJ, 141, 16
Johnson J. A. et al., 2011b, ApJS, 197, 26
Jura M., 2008, AJ, 135, 1785
Kains N., Wyatt M. C., Greaves J. S., 2011, MNRAS, 414, 2486
Kalas P., Graham J. R., Beckwith S. V. W., Jewitt D. C., Lloyd J. P., 2002, ApJ, 567, 999
Kalas P., Graham J. R., Clampin M., 2005, Nature, 435, 1067
Kalas P. et al., 2008, Science, 322, 1345
Kennedy G. M. et al., 2012a, MNRAS, 421, 2264
Kennedy G. M., Wyatt M. C., Sibthorpe B., Phillips N. M., Matthews B. C., Greaves J. S., 2012b, MNRAS, 426, 2115
Koester D., Girven J., Gänsicke B. T., Dufour P., 2011, A&A, 530, A114
Kóspál Á., Ardila D. R., Moór A., Ábrahám P., 2009, ApJ, 700, L73
Krivov A. V. et al., 2013, ApJ, 772, 32
Lagrange A., Desort M., Galland F., Udry S., Mayor M., 2009, A&A, 495, 335
Lloyd J. P., 2011, ApJ, 739, L49
Lloyd J. P., 2013, ApJ, 774, L2
Löhne T., Krivov A. V., Rodmann J., 2008, ApJ, 673, 1123
Marois C., Macintosh B., Barman T., Zuckerman B., Song I., Patience J., Lafrenière D., Doyon R., 2008, Science, 322, 1348
Matthews B. C. et al., 2010, A&A, 518, L135
Melis C., Jura M., Albert L., Klein B., Zuckerman B., 2010, ApJ, 722, 1078
Mermilliod J.-C., 1987, A&AS, 71, 413
Morel M., Magnenat P., 1978, A&AS, 34, 477
Moro-Martín A. et al., 2007, ApJ, 658, 1312
Moshir M. et al., 1993, VizieR Online Data Catalog, 2156, 0
Ott S., 2010, in Mizumoto Y., Morita K.-I., Ohishi M., eds, ASP Conf. Ser. Vol. 434, Astronomical Data Analysis Software and Systems XIX. Astron. Soc. Pac., San Francisco, p. 139
Perryman M. A. C., ESA, 1997, ESA SP-1200: The Hipparcos Catalogue. ESA, Noordwijk
Phillips N. M., Greaves J. S., Dent W. R. F., Matthews B. C., Holland W. S., Wyatt M. C., Sibthorpe B., 2010, MNRAS, 403, 1089
Poglitsch A. et al., 2010, A&A, 518, L2
Rameau J. et al., 2013, ApJ, 772, L15
Raymond S. N., Scalo J., Meadows V. S., 2007, ApJ, 669, 606
Rieke G. H. et al., 2005, ApJ, 620, 1010
Sato B. et al., 2010, PASJ, 62, 1063
Schlaufman K. C., Winn J. N., 2013, ApJ, 772, 143
Sibthorpe B., Ivison R. J., Massey R. J., Roseboom I. G., van der Werf P. P., Matthews B. C., Greaves J. S., 2013, MNRAS, 428, L6
Smith R., Churcher L. J., Wyatt M. C., Moerchen M. M., Telesco C. M., 2009, A&A, 493, 299
Su K. Y. L. et al., 2006, ApJ, 653, 675
Trilling D. E. et al., 2008, ApJ, 674, 1086
Valenti J. A., Fischer D. A., 2005, ApJS, 159, 141
Wyatt M. C., 2008, ARA&A, 46, 339
Wyatt M. C., Clarke C. J., Greaves J. S., 2007a, MNRAS, 380, 1737
Wyatt M. C., Smith R., Greaves J. S., Beichman C. A., Bryden G., Lisse C. M., 2007b, ApJ, 658, 569
Wyatt M. C., Smith R., Su K. Y. L., Rieke G. H., Greaves J. S., Beichman C. A., Bryden G., 2007c, ApJ, 663, 365
Wyatt M. C. et al., 2012, MNRAS, 424, 1206
Zuckerman B., Melis C., Klein B., Koester D., Jura M., 2010, ApJ, 722, 725

This paper has been typeset from a TEX/LATEX file prepared by the author.